BIOCHEMISTRY
including biophysical chemistry & molecular biology

Article

pubs.acs.org/biochemistry

Importance of Domain Closure for the Autoactivation of ERK2

Daniel Barr,[†,∥] Taiji Oashi,[‡] Kimberly Burkhard,[‡] Sarah Lucius,[†] Ramin Samadani,[‡] Jun Zhang,[‡] Paul Shapiro,*[,‡] Alexander D. MacKerell, Jr.,*[,‡] and Arjan van der Vaart*[,§]

[†]Department of Chemistry and Biochemistry, Center for Biological Physics, Arizona State University, P.O. Box 871604, Tempe, Arizona 85287, United States

[‡]Department of Pharmaceutical Sciences, University of Maryland, 20 North Pine Street, Baltimore, Maryland 21201, United States

[§]Department of Chemistry, University of South Florida, 4202 East Fowler Avenue CHE 205, Tampa, Florida 33620, United States

Supporting Information

ABSTRACT: Extracellular signal-regulated kinases 1 and 2 (ERK1 and -2, respectively) play a critical role in regulating cell division and have been implicated in cancer. In addition to activation by MAPK/ERK kinases 1 and 2 (MEK1 and -2, respectively), certain mutants of ERK2 can be activated by autophosphorylation. To identify the mechanism of autoactivation, we have performed a series of molecular dynamics simulations of ERK1 and -2 in various stages of activation as well as the constitutively active Q103A, I84A, L73P, and R65S ERK2 mutants. Our simulations indicate the importance of domain closure for autoactivation and activity regulation, with that event occurring prior to folding of the activation lip and of loop L16. Results indicate that the second phosphorylation event, that of T183, disrupts hydrogen bonding involving D334, thereby allowing the kinase to lock into the active conformation. On the basis of the simulations, three predictions were made. G83A was suggested to impede activation; K162M was suggested to perturb the interface between the N- and C-domains leading to activation, and Q64C was hypothesized to stop folding of loop L16, thereby perturbing the homodimerization interface. Functional analysis of the mutants validated the predictions concerning the G83A and Q64C mutants. The K162M mutant did not autoactivate as predicted, however, which may be due to the location of the residue on the protein surface near the ED substrate docking domain.

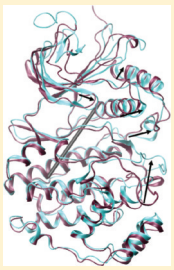

Mitogen-activated protein kinases (MAPKs) form a regulatory signal cascade that controls cell proliferation.[1−3] Growth signals (mitogens) are recognized in the extracellular environment by surface receptors, which then activate a signal cascade to amplify and transmit the growth signal to the nucleus, initiating cell proliferation. Because of their critical role in regulating cell proliferation, mutations in many of these kinases have been implicated in a variety of human diseases, especially cancer. The Ras/Raf/MEK/ERK (or MAPK) signaling pathway is particularly important in this regard, as ∼30% of all human cancers involve mutations in the Ras genes.[4−6] Consequently, MAPK signaling has become a prominent area of study for drug development, and targets include the extracellular signal-regulated kinases (ERK).[7−13]

The ERK consist of two isoforms (ERK1 and ERK2), with 90% identical sequences. ERK1 and -2 have been implicated in human cancers[14] as well as Alzheimer's disease[15] and dwarfism.[16] ERK1 and -2 are activated by phosphorylation at two conserved residues on the activation lip, T183 and Y185 (numbering as in rodent ERK2).[17] The two phosphorylation events (mediated by MEK1 and -2) are not simultaneous, but they are cooperative and occur in quick succession, with phosphorylation occurring first at the tyrosine residue and then at the threonine.[18−20] Upon activation, ERK proteins may form homodimers and be targeted to the nucleus, where they phosphorylate transcription factors responsible for cell proliferation and differentiation.[21,22]

Structural studies of ERK2 have identified several substrate binding sites and conformational dynamics involved in the activation and regulation of the kinase.[17,23,24] The binding sites and other important structural elements of the protein are shown in Figure 1a, while structural differences between the active and inactive states are shown in Figure 1b. The ED (residues 157 and 158) and CD sites (residues 316−319) are responsible for substrate binding and specificity.[25,26] In addition, allosteric sites that impact the activation or function of ERK1 and -2 such as the DFG (residue 165−167) and DEF (residues 231−235 and 255−261) sites have been identified,[12,13,27] suggesting the importance of long-range dynamic effects for activation. Phosphorylation displaces the activation lip, with many of the residues in the lip moving by as much as 10 Å (Figure 1b).[17] Other structural changes upon activation include the folding of a 3_{10} helix at loop L16, which exposes a hydrophobic zipper that forms the domain interface in the dimer,[21] and a small domain closure in which the N-domain rotates 5° over the C-domain.[17] In a recent structure of monophosphorylated ERK1 (phosphorylated only at the tyrosine; no such structure is available for ERK2), domain closure has occurred, but no conformational changes were observed in the activation lip or loop L16.[24] Because monophosphorylated ERK1 has a basal activity (∼500-fold lower than that of the fully active form),[24] this observation suggests that domain closure is important for kinase activity.

In addition to activation by MEK, certain mutations will activate ERK2 through an autoactivation mechanism.[28,29] This

Received: April 4, 2011
Revised: July 29, 2011
Published: August 15, 2011

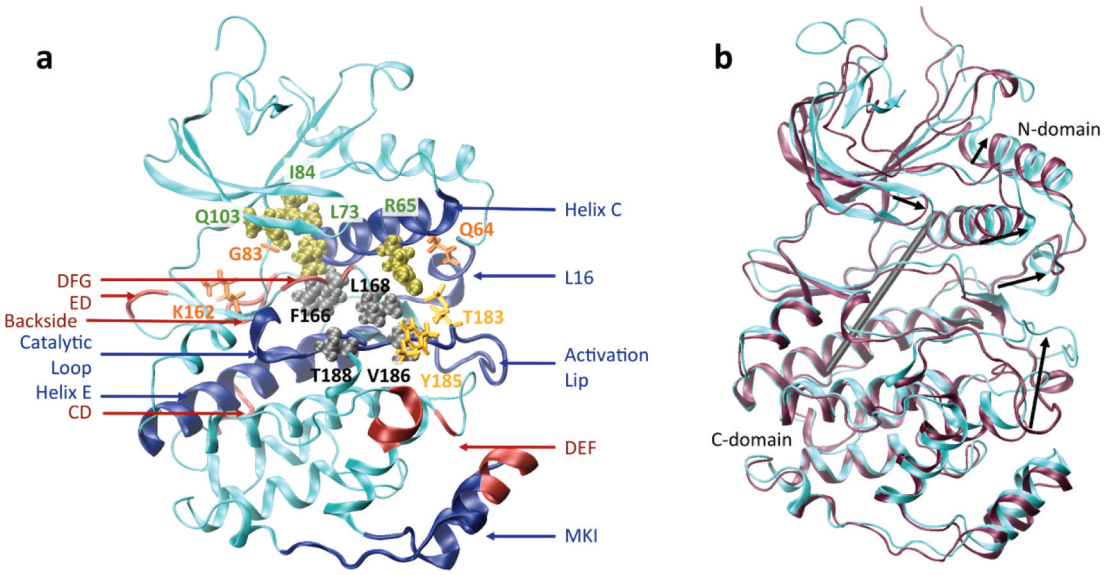

Figure 1. (a) Crystal structure of active ERK2.[17] Important structural elements and binding sites are colored blue and red, respectively. The phosphorylated T183 and Y185 residues are colored yellow. The F166, L168, V186, and T188 residues of the hydrophobic pathway are shown as black spheres. Q103, I84, L73, and R65 are shown as green spheres and important for autoactivation. Q64, G83, and K162 are colored orange; mutants of these residues were proposed and tested in this study. (b) Crystal structure of inactive[23] (magenta) and active[17] (cyan) ERK2. The major structural changes upon activation are indicated with arrows, showing the refolding of the activation lip, the folding of the L16 loop, and the rotation of the N-domain. The hinge axis for rotation is indicated and corresponds to the dihedral angle along helices C and E.

mechanism involves the gatekeeper residue Q103 and adjacent hydrophobic residues I84 and L73 (Figure 1a). Mutation of these hydrophobic residues to smaller residues (Gly or Ala) led to enhanced autophosphorylation and kinase activity.[28] It is thought that the gatekeeper I84 and L73 residues are connected to the activation lip by a "hydrophobic spine", consisting of residues F166, L168, and V186 and T188 in the lip (Figure 1a).[28] The existing model predicts that regulation of protein flexibility over long distances is central to the autoactivation mechanism of the mutants. It is thought that the mutants lead to an increased flexibility of the activation lip, which would ease autophosphorylation.[28]

Here we present a series of molecular dynamics (MD) simulations to further investigate the autoactivation mechanism of ERK2. Our studies examine the dynamics of the autoactivated mutants,[28] in which the gatekeeper and hydrophobic spine residues are mutated to smaller residues. We studied the Q103A, I84A, and L73P mutants, as well as the active and inactive states of ERK2, and monophosphorylated ERK1. We also studied the autoactivated R65S mutant, which is constitutively active, but for which the autoactivation mechanism is unclear.[29] A main goal of our simulations was to test whether the mutants display increased atomic fluctuations of the activation lip as predicted in the existing model.[28] To our surprise, no such increases were observed in the simulations. Instead, our analyses suggest that the mutations induce domain closure, which might lead to autoactivation. On the basis of the calculations, it was predicted that residues G83, K162, and Q64 are involved in the activation mechanism. Accordingly, the following mutants, G83A, K162M, and Q64C, were expressed and tested in biological experiments. Consistent with the predictions, the G83A mutant disrupted the ability of ERK2 to phosphorylate MBP. The Q64C mutant also showed behavior consistent with the predictions, as it displayed an inability to form homodimers. The K162M mutant did not result in the predicted decrease in ERK2 activity, however, which might be due to its proximity to the ED binding site.

MATERIALS AND METHODS

Molecular Dynamics Simulations. All simulations were performed with CHARMM[30] and NAMD.[31] Analyses were performed with CHARMM[30] and MDAnalysis;[32] structures were visualized with VMD,[33] and secondary structure elements were calculated with STRIDE.[34]

The structures of inactive[23] and active[17] ERK2 and monophosphorylated ERK1[24] were obtained from the Protein Data Bank (entries 1ERK, 2ERK, and 2ZOQ, respectively) and solvated in a box of TIP3P water[35] sized to extend a minimum of 12 Å beyond protein non-hydrogen atoms with potassium ions to neutralize the charge of the system. Structures of ERK2 mutants L73P, I84A, Q103A, R65S, K162M, and G83A were modeled on the basis of the inactive structure[23] and solvated in a box of TIP3P water sized to extend a minimum of 10 Å beyond protein non-hydrogen atoms with 150 mM NaCl. After being minimized and heated, the systems were equilibrated for 500 ps while being looped over decreasing restraints on the protein backbone. This was followed by unrestrained MD equilibration for 5 ns and a 20 ns production run (30 ns for the mutants). The simulations were performed in the NPT ensemble at 1 atm and 300 K using the CHARMM22 all-atom protein force field[36] with the CMAP correction.[37] SHAKE[38] was applied to constrain bonds involving hydrogen, and a 2 fs time step was used. Electrostatic forces were calculated with the particle mesh Ewald method[39] using a real space cutoff of 12 Å with a κ of 0.4 Å^{-1}. van der Waals forces were truncated with a switching function between 10 and 12 Å. Snapshots were saved every 1 ps; the last 20 ns of the simulations was used for the analysis.

Domain closure was calculated as the dihedral angle between the helix axes of helices C and E; averages and standard

dx.doi.org/10.1021/bi200503a | *Biochemistry* 2011, 50, 8038–8048

deviations were calculated, and comparisons between the simulations were made using a mean difference test with a zero mean null hypothesis. Hydrogen bonds were calculated using a distance cutoff of 3 Å and a minimum lifetime of 10 ps. Solvent accessible surface areas were calculated using a probe radius of 1.4 Å. A sequence alignment of MAPKs to assess the conservation of residues was created using ClustalW2.[40]

The variance−covariance matrices and quasi-harmonic modes were obtained by standard means;[41−43] correlated motions were also quantified by a mutual information analysis,[44] implemented using the methodology described in ref 45. A block analysis[46] was performed to assess the convergence of the root-mean-square deviations (rmsd) of each of the simulations. Convergence was calculated by dividing the trajectory into blocks (a range of values between 2 and 500 blocks was used); the rmsd was calculated for each block, and the standard deviation was calculated over all of the blocks. The standard deviation is plotted as a function of the reciprocal of the number of frames in each block (Figure S1a of the Supporting Information). Convergence of the variance−covariance matrices was assessed using the equation $R(t) = [\mathbf{C}(t) - \mathbf{C}(t-N\tau)]^2/N_{res}$, where N_{res} is the number of residues, $\mathbf{C}(t)$ is the variance−covariance matrix for the full trajectory, and $\mathbf{C}(t-N\tau)$ is the covariance matrix calculated for a trajectory shortened by N multiples of τ (Figure S1b of the Supporting Information).[47] The value of $R(t)$ was obtained as the average of 75 different trajectory reshufflings using a τ of 100 ps; upon convergence, $R(t) \rightarrow 0$. In all cases, satisfactory convergence for the rmsd and variance−covariance matrix was obtained.

To quantify information flow in the system, we performed a transfer entropy analysis on each trajectory.[45] In this method, the C^α atomic fluctuations of each residue i $[r_i(t)]$ are stored as state vectors $\mathbf{I}_k$ and $\mathbf{I}_{k+1}$. Taking time $t_{k+(m-1)\tau}$ as the present, the history of the atomic fluctuations is given by $\mathbf{I}_k = [r_i(t_k), r_i(t_{k+\tau}), ..., r_i(t_{k+(m-1)\tau})]$ and the future fluctuations are given by $\mathbf{I}_{k+1} = r_i(t_{k+m\tau})$. The time delay τ and embedding dimension m are chosen such that the dynamical structure of the time series is preserved.[45] Transfer entropy $T_{j\rightarrow i} = \mathbf{I}(\mathbf{I}_{k+1};\mathbf{J}_k|\mathbf{I}_k)$ is the conditional mutual information between $\mathbf{I}_{k+1}$ and $\mathbf{J}_k$ and quantifies the amount of information that knowing the history of the fluctuations of j provides the future fluctuations of i, given the history of i. Because transfer entropies are nonsymmetrical ($T_{j\rightarrow i} \neq T_{i\rightarrow j}$), they can be used to measure the direction of information flow. This is most conveniently done using the index $D_{j\rightarrow i} = T'_{j\rightarrow i} - T'_{i\rightarrow j} \in [-1,1]$, where $T'_{j\rightarrow i}$ is the normalized transfer entropy between j and i. If $D_{j\rightarrow i}$ is positive, information is flowing from j to i (j is the source); thus, the fluctuations of atom j drive the future fluctuations of atom i. If $D_{j\rightarrow i}$ is negative, information flows from i to j (j is a sink), and on average, j responds to the motion of i.

Transition pathways for unphosphorylated ERK2 were calculated using the original and restricted perturbation targeted MD methods (TMD[48] and RP-TMD,[49] respectively) to pull the system from the inactive to the active state. To generate a multitude of pathways, these simulations were performed with the FACTS implicit solvent model,[50] which significantly decreased the cost of the simulations (because of the smaller number of simulated particles and the absence of friction and relaxation processes associated with the displacement of water molecules while the protein undergoes its change in shape). To test the quality of the implicit solvent simulations, we also performed a TMD simulation in explicit water with CHARMM and a restrained TMD simulation in explicit water with NAMD.[31] The latter method uses a restraint rather than a constraint for the targeting. The implicit solvent TMD simulations decreased the rmsd with the target by 1.0×10^{-5} Å at each MD step, reaching a final rmsd of 0.5 Å after 600 ps; a total of 25 simulations were performed. Five implicit solvent RP-TMD simulations were performed with maximum atomic perturbations p_F ranging from 1.0×10^{-5} to 2.0×10^{-3} Å and 25 with a p_F of 5.0×10^{-5} Å; in each case, the reverse perturbation $p_R = 0.5p_F$. The implicit solvent simulations used Langevin dynamics with a damping coefficient of 40 ps $^{-1}$, a heat bath of 300 K, a constant dielectric of 1.0, a switching function between 10 and 12 Å for the van der Waals forces, SHAKE[38] for bonds involving hydrogen atoms, and a 2 fs time step. The explicit solvent TMD simulation decreased the rmsd by 5.0×10^{-7} Å at each time step; the restrained TMD simulation used a force constant of 200 kcal mol^{-1} Å^{-2}. The additional setup of the explicit water runs was identical to that of the explicit water MD simulations.

ERK2 Mutations. ERK2 mutagenesis was conducted by polymerase chain reaction using the QuikChange XL Site-Directed Mutagenesis Kit from Stratagene (La Jolla, CA). The following oligonucleotides were purchased from Integrated DNA Technologies (Coralville, IA) and used without further purification for generating the G83A, K162M, and Q64C mutations: G83A forward, 5′GACATGAGAACATCATCGCCATCAATGACATCATCCG3′; G83A reverse, 5′CGGATGATGTCATTGATGGCGATGATGTTCTCATGTC3′; K162M forward, 5′CACCACTTGTGATCTCATGATCTGTGAXCTTTGGCC3′; K162M reverse, 5′GGCCAAAGTCACAGATCATGAGATCACAAGTGGTG3′; Q64C forward, 5′AGTCCTTTTGAGCACCAGACCTACTGTTGCAGAACCCTGAGAGA3′; Q64C reverse, 5′TCTCTCAGGGTTCTGCAACAGTAGGTCTGGTCAAAAGGACT3′. All mutations were verified by DNA sequencing at the Biopolymer Laboratory, School of Medicine, University of Maryland.

ERK2 wild type and mutants were expressed as N-terminally His_6-tagged proteins in *Escherichia coli* BL21(DE3) in LB medium. A single colony was inoculated in LB medium containing 100 μg/mL ampicillin and incubated overnight at 37 °C with shaking. The overnight culture was diluted 100-fold in fresh medium, cultured at 30 °C to an optical density of 0.8 at 600 nm, and then induced with 1 mM isopropyl D-1-thiogalactopyranoside for 3 h (wild type and K162M mutant) or 6 h (G83A and Q64C mutants). Cells were collected by centrifugation, and the pellet was resuspended in BugBuster (EMD Biosciences, San Diego, CA) containing 10% (w/v) glycerol, 1 mM PMSF, and Complete Mini EDTA-free protease inhibitor cocktail (Roche Diagnostics). Cells were sonicated on ice using a Sonicator 3000 Ultrasonic Liquid Processor (Misonix) and lysates centrifuged at 18000*g* for 45 min at 4 °C. The supernatant was loaded onto a Ni-NTA column (Qiagen), pre-equilibrated with 300 mM NaCl and 50 mM phosphate buffer (pH 7.5), and washed with 10 column volumes of 300 mM NaCl, 50 mM phosphate buffer (pH 7.5), and 20 mM imidazole. Proteins were eluted with 300 mM NaCl, 50 mM phosphate buffer (pH 7.5), and 250 mM imidazole, concentrated using an Amicon Ultra-15 Centrifugal Filter Device (Millipore), and desalted into buffer containing 100 mM NaCl and 50 mM phosphate buffer (pH 7.5) by using an Econo-Pac P6 cartridge (Bio-Rad). The protein was further purified with a Q Sepharose Fast Flow ion exchange column (Sigma-Aldrich) utilizing a 50

to 500 mM NaCl gradient and a S200 size exclusion column (GE Healthcare) sequentially to further purify the protein. The resulting protein was then concentrated to a final concentration of 6 mg/mL in storage buffer containing 200 mM NaCl and 50 mM Tris-HCl (pH 7.5). Purified protein was aliquoted and stored at −80 °C. The constitutively active (CA) MKK1 His_6 construct was kindly provided by K. Dalby (University of Texas, Austin, TX) and prepared as previously described.[51]

In in vitro kinase assays, ERK2 wild type or mutant proteins (5 μg) with 0.5 μg of myelin basic protein (MBP) were incubated in the presence or absence of CA MKK1 for 2−60 min at 30 °C in 50 mM Tris-HCl, 10 mM $MgCl_2$, 1 mM EGTA, 2 mM DTT, and 0.01% Brij 35 (pH 7.5) containing 20 μM ATP and 2 μCi of [γ-^{32}P]ATP in a 20 μL volume. Reactions were stopped by adding an equal volume of 2× sodium dodecyl sulfate−polyacrylamide gel electrophoresis (SDS−PAGE) sample buffer, and the proteins were separated by SDS−PAGE. The gels were stained with Coomassie blue and dried, and the incorporation of ^{32}P into ERK2 and MBP was assessed by phosphoimager analysis.

For native gel electrophoresis, a precast 4 to 15% Tris-HCl−polyacrylamide native gel (Bio-Rad) was equilibrated in Tris-glycine running buffer for 4 h. After equilibration, 5 μg of wild-type and mutant Q64C in 2× native loading dye were loaded on the gel and subjected to electrophoresis for 6 h at 5 mA and 25 V. The gel was then stained with Coomassie blue for evaluation of oligomeric structures.

For immunoblotting, proteins were separated by SDS−PAGE and detected following immunoblotting using enhanced chemiluminescence (ECL, GE Healthcare). Primary antibodies against ERK2 or phosphorylated ERK1 and -2 were purchased from Santa Cruz Biotechnology (Santa Cruz, CA) or Sigma, respectively.

RESULTS

Atomic Fluctuations in the Hydrophobic Spine and Lip Are Not Increased in ERK2 Mutants. On the basis of the experimental predictions,[28] we expected to observe increased atomic fluctuations of residues near the DFG site (residues 165−167) and the lip. Analysis of the rmsf for this region showed relatively small differences between the mutants and the inactive state, however (Figure 2). Moreover, regions of the lip with slight increases in flexibility differed among all mutants, and for portions of the lip, the fluctuations for the mutants were actually smaller than for the inactive state. Mutant L73P showed slightly more flexibility on the N-terminal side of T183/Y185 (residues 174−179); Q103A showed increased flexibility around T183/Y185 (residues 182−185), and I84A showed enhanced flexibility on the C-terminal end of the lip (residues 186−190) compared to the inactive state. The monophosphorylated state showed diminished fluctuations relative to both the active and inactive states for residues 174−179 but slightly increased fluctuations toward the C-terminal end of the lip. Consistent with the small changes in the number of fluctuations, the solvent accessible surface area of Y185 in the mutants showed small differences with that of the inactive state (Table T1 of the Supporting Information). The mutants became slightly more solvent exposed, but because the differences were only a few square angstroms, the effect was not significant. None of the six trajectories demonstrated large backbone fluctuations in the DFG region. A comparison of the rotamer distributions of the side chains of these residues revealed no increased flexibility of the hydrophobic side chains in the mutant simulations (data not shown). These results indicate that the mutations do not lead to significantly increased fluctuations in the hydrophobic spine or activation lip.

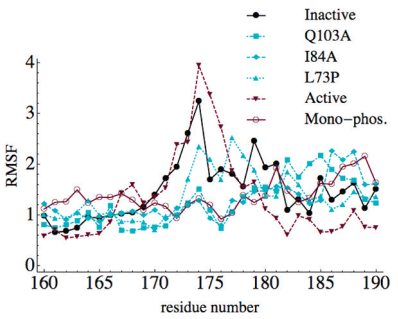

Figure 2. Root-mean-square fluctuations for residues 160−190 (the DFG site through the activation lip). Monophos. refers to the monophosphorylated state of ERK1; all other data are for ERK2.

Table 1. Domain Closure Calculated as the Dihedral Angle along Helices C and E (see Figure 1B)

system	MD average closure angle (deg)	X-ray average closure angle (deg)
inactive[a]	82.5 ± 3.8	80.4
Q103A[a]	88.2 ± 2.7	
I84A[a]	84.6 ± 2.7	
L73P[a]	88.6 ± 2.9	
R65S[a]	87.7 ± 2.0	
G83A[a]	83.0 ± 3.3	
K162M[a]	83.3 ± 3.7	
monophosphorylated[b]	93.2 ± 1.9	90.7
active[a]	89.1 ± 2.7	86.0

[a]ERK2. [b]ERK1.

Domain Closure Is Observed in All States but Inactive ERK2. Domain closure was observed in all states except for the inactive kinase (Table 1). In each of the mutants, domain closure happened early in the simulation (during equilibration) and was preserved throughout the entire trajectory. This is notable given that the mutant simulations were initiated from the inactive state. In the I84A simulation, the closure was intermediate between the active and inactive states, while in the other mutants, the closure was complete. Of the three structural changes associated with activation of the kinase [domain closure, refolding of the lip, and folding of loop L16 (see Figure 1b)], domain closure was the only one that was observed consistently throughout our simulations. Loop L16 showed intermediate behavior in most of the simulations, with it curling up toward helix C in the mutants and monophosphorylated state. L16 never sampled the fully folded state in any trajectory except the active state; in the Q103A mutant, a partial folded state was reached. Throughout our simulations, with the exception of the active state, the lip remained folded down in the inactive conformation during the entire trajectory. These results suggest that domain closure is the first of the three major structural changes to occur during autoactivation of the kinase.

dx.doi.org/10.1021/bi200503a | Biochemistry 2011, 50, 8038−8048

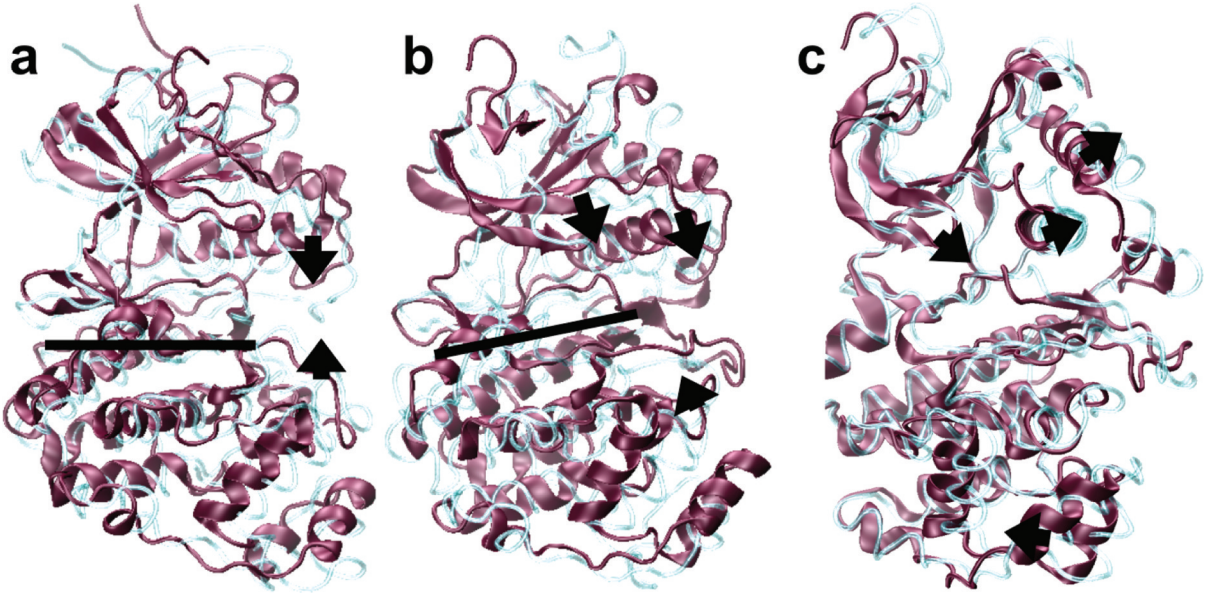

Figure 3. Quasi-harmonic modes of ERK2. The protein oscillates between the magenta and cyan structures; arrows indicate important motions, and the hinge axis is shown as a black line. (a) Hinge bending motion in the inactive state. (b) Hinge bending motion in the active state. The 5° rotation of the axis in the active state realigns the hinge axis so that the hinge motion is oriented over the ATP binding site and along the substrate binding groove. (c) Quasi-harmonic mode 14 from the active state trajectory showing the domain rotation. The N- and C-terminal domains rotate in opposite directions.

Quasi-harmonic analyses of the inactive and active states showed that hinge-type compression over the substrate binding site and ED motif was a dominant motion for activation (Figure 3a,b; also shown as movies M1 for the inactive and M2 for the active state in the Supporting Information). This mode (mode 16 for the inactive, mode 13 for the active state; in the numbering of modes, the first six zero-frequency modes are ignored) contained 8 and 12% of the total motion in the inactive and active states, respectively. Inspection of this hinge motion revealed a small shift of the hinge axis upon activation. In the inactive state, several quasi-harmonic modes involved the upward movement of the activation lip, rotation of helix C, and lowering of the L16 loop. These modes show strong motions toward the active state conformation. In most cases, these were not the modes representing the largest amplitude motions, but they could be observed within the 20 lowest-frequency non-zero modes and together account for 13% of the total variance in the trajectory. Other notable modes that represent potentially biologically relevant motions include mode 2 in the inactive state that involves a closing of helix C and the N-domain over the C-domain. Modes 4 and 16 show strong upward movement of the activation lip and a corresponding downward movement of loop L16.

The active state had one low-frequency mode (mode 14) that did not have a corresponding motion in the inactive state: an asymmetric twisting motion, in which the N-domain rotated over the C-domain, the backside binding site (residues 78−81) moving down toward the ED site, and the MAP kinase insertion (MKI) rotated out away from the active site and toward helix G (Figure 3c; also shown as movie M3 in the Supporting Information). Another active state mode (mode 20) showed strong downward motion of the $\beta1-\beta2$ loop over the ATP binding site and the catalytic loop and might be important for catalysis.

Motion of Residues Is More Strongly Coupled in the Inactive State. Analysis of variance−covariance matrices, which provide information about the extent of correlation of motions of residues, showed that the correlations in the active and inactive states are generally equal in sign but different in magnitude. To ease the comparison, the variance−covariance matrices for the active and inactive state are shown as one matrix in Figure 4, by using the lower triangular part for the active state and the upper triangular part for the inactive state. Overall, the active state had much weaker correlations than the inactive state (see also Table T2 of the Supporting Information). In particular, the various binding sites were much more strongly coupled in the inactive state. For example, activation led to a significant loss of correlation between the ERK2 MKI helices (residues 244−267, which may serve as a nuclear locator sequence[21]) and the rest of the protein, as well as a significant decoupling of the activation lip from the rest of

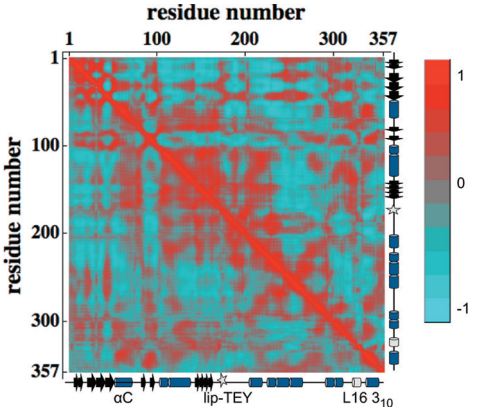

Figure 4. Variance−covariance matrix of the inactive (upper triangular part) and active state (lower triangular part). Structural elements are indicated along the axis; the phosphorylation site (TEY motif) is shown as a light gray star, and the 3_{10} helical region of L16 in the active state is colored light gray.

dx.doi.org/10.1021/bi200503a | *Biochemistry* 2011, 50, 8038−8048

the protein (Table T2 of the Supporting Information). In the active state, the correlation between the activation lip and the DEF site was lost. Activation changed the correlation between the activation lip and the backside binding site (residues 78−82) from negative (out-of-phase) to positive (in-phase); mutual information analysis also showed that correlations between these regions decreased upon activation. The mutual information indicated a strong correlation between the DFG-out site and the N-domain in the inactive state, which was greatly reduced in the active state. The latter observation might indicate that inhibitors binding to the DFG site of the related p38 MAP kinase[52] also affect the dynamics of the N-domain, possibly affecting domain closure. Strong correlations among the ED site (residues 157 and 158), the ATP binding residues, and the backside binding site also decreased upon activation. Little correlation was found between the ED and CD binding sites, indicating that these two docking groove binding sites can operate independently.[25,53]

The ERK2 mutants and ERK1 monophosphorylated state showed the same general correlation patterns as the ERK2 wild-type inactive and active states, with magnitudes often intermediate between the active and inactive states (Figure S2 and Table T2 of the Supporting Information). The correlations of the Q103A mutant were very similar to those of the inactive state, except that correlations with residues 328−335 (the L16 region that refolds into a 3_{10} helix in the active state) were similar to those of the active state. Correlations in the I84A mutant were mostly similar to those of the inactive state, with stronger correlations between regions involving the DEF site and C helix and significantly weaker correlations between the activation lip and the rest of the protein. The L73P mutant showed the weakest correlations of all of the mutant trajectories, the loss of correlation being most evident between the activation lip and the MKI and DEF site; residues 328−335 showed diminished correlation with the rest of the protein. The monophosphorylated state showed coupling patterns containing certain aspects seen in both the active or inactive states. The activation lip maintained a high magnitude of correlation with the rest of the protein as in the inactive state, though the sign of the correlation was positive as in the active state. The correlations between the MKI and DEF sites and the N-domain were similar to those of the active state, with a significant decoupling of motion, particularly for helix C.

The overall similarity of correlation patterns demonstrates a certain dynamical robustness of the protein, consistent with the fact that more than 90% of the residues move <2 Å upon activation.[17] The higher magnitude of correlations in the inactive state suggests that the motions of distant elements of the protein in the inactive state are more strongly coupled than in the other states; notably, the various binding sites are much more strongly coupled in the inactive state. The stronger coupling might facilitate the communication of events through the protein to achieve the active state.

The transfer entropy patterns were also very similar for all states. Upon activation, only 15% of the residues change from driver to responder, and vice versa. More than half of these changes involved the L16 loop, which became a source (or driver of correlated motions) upon activation. Helix C switched from an overall source in the inactive state to a sink (or responder) in the active state, while the activation lip generally drove the correlations in both the active and inactive states. In all states, the ATP-binding residues, the N-terminal helices, and the C-terminal residues were sources of information flow. The transfer entropy of the monophosphorylated state was very similar to that of the inactive state, which indicates that domain closure is not sufficient to change the pattern of information flow in the protein without the corresponding refolding of the lip.

The mutant simulations also showed transfer entropy patterns most similar to those of the inactive state, though with a few interesting exceptions. In the Q103A mutant, the L16 loop and the DFG site were more driving than in the inactive state, which is consistent with our observation of partial refolding of the L16 loop during that simulation. In the I84A mutant, we observed stronger driving of the C helix and weaker driving of the activation lip than in the inactive state. The L73P mutant showed driving behavior of the activation lip and the L16 loop stronger than that observed in the inactive state, but not as strong as what was observed in the active state.

The Second Phosphorylation Locks the Domain-Closed State and Opens the Dimerization Interface. Structural comparisons of the active and inactive state simulations revealed networks of hydrogen bonds that stabilize the active state. These networks are centered on the phosphorylated residues and also involve helix C and loop L16. In the inactive state, loop L16 remained folded down, allowing D334 to form strong hydrogen bonds with R170 and R68 but making only a weak contact with Q64. As loop L16 began to refold, seen most clearly in the L73P and Q103A mutants and the monophosphorylated state, D334 moved up and farther from the activation lip. This motion weakened its contact with R68 but strengthened its contact with Q64. In the active state, the lip and loop L16 completely refolded, such that R170 made a strong hydrogen bond with pT183 instead of D334. In addition, R68 hydrogen bonds to pT183. As this happened, D334 rotated up to make a strong contact with Q64, locking helix C into the active conformation. With loop L16 completely refolded, a hydrogen bond contact between D334 and the backbone of R68 is restored that was weakened in the intermediately folded state. This contact network is shown in Figure 5 for the inactive state, the Q103A mutant, and the active state. Distance histograms for D334 in the inactive, active, and Q103A simulations are shown in Figure S3 of the Supporting Information.

The critical role of the second phosphorylation event for locking in domain closure can also be inferred from contacts involving R68 and R170. Until the activation lip refolds, R68 and R170 contact D334 and prevent loop L16 from folding upward toward helix C. When pT183 refolds, it displaces D334 and allows refolding of loop L16. Mediated by the Q64−D334 contact, the refolded L16 loop restricts the flexibility of helix C, preventing the overclosed conformation observed in the monophosphorylated state of ERK1 (see Table 1) and locking the domain closure in the active state conformation.

The refolding of the L16 loop also causes the hydrophobic zipper region to become accessible. This region forms the homodimerization interface,[21] which is required for full enzyme activity. Given the significant structural change that the L16 loop undergoes and the important role the simulations indicate that Q64 plays in that restructuring, it was hypothesized that mutation of this residue would disrupt dimerization by removal of the Q64−D334 contact. Although Q64 is not well-conserved in the ERK family or among tyrosine kinases in general (Figure S4 of the Supporting Information), our simulations indicated that this residue might be critical for ERK2. Consequently, we postulated that a Q64C mutation would significantly weaken

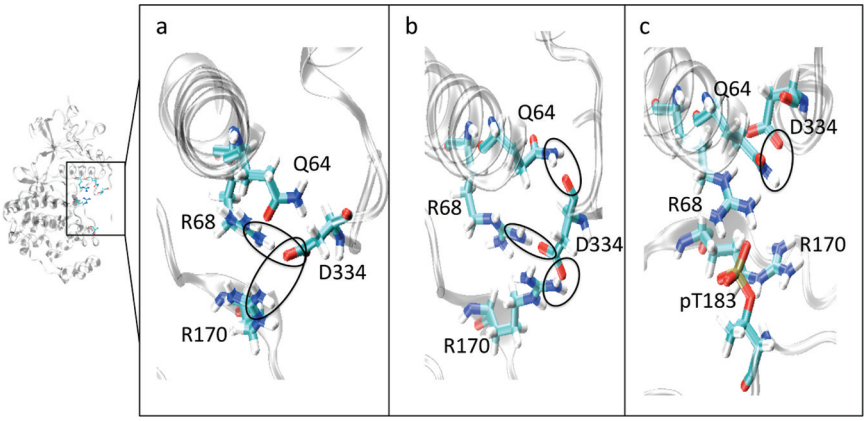

Figure 5. Close-up of the contact network for (a) the inactive state, (b) the Q103A mutant, and (c) the active state. In the inactive state, R68 and R170 contact D334, preventing refolding of loop L16. The Q103A mutant shows the transition in the contact network as loop L16 begins to refold, strengthening the contact between D334 and Q64. In the active state, pT183 has refolded upward to contact R68 and R170, allowing D334 to fold upward to make a stronger contact with Q64 and lock in the domain closure. Ovals highlight the contacts made by D334 in each structure.

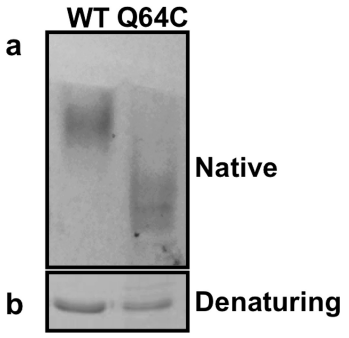

Figure 6. Altered migration of the ERK2 Q64C mutant in native gels. ERK2 wild type and Q64C were electrophoresed by (a) native nondenaturing gels or (b) denaturing SDS–PAGE. Proteins were stained with Coomassie blue, destained, and photographed.

the interactions with D334 and disrupt the formation of the dimerization interface. The Q64C mutant was generated and compared to ERK2 wild type using a native nondenaturing acrylamide gel. It was predicted that migration through the native gel would be faster for the Q64C mutant if dimerization was affected. Indeed, these experiments showed that the Q64C mutation did affect ERK2 migration in the native gel as compared to that of the wild type, indicating that ERK2 dimerization and/or oligomerization was weakened (Figure 6). However, on denaturing gels, the ERK2 wild-type and Q64C proteins showed similar migration patterns (Figure 6).

Targeted Molecular Dynamics Simulations Show Early Domain Closure. TMD simulations were undertaken to better characterize the conformational transition from the inactive to active state of ERK2. All of our TMD and RP-TMD simulations revealed that domain closure occurs early in the activation pathway, before the other structural changes are complete (Table 2). Initially, the domain closure proceeded beyond the active state value by ~10° (115%), reaching closure angles similar to those of monophosphorylated ERK1, but as the activation lip refolded, the domain closure shifted back to the active state value. The maximum value of the domain closure occurred when refolding of the activation lip was 44% complete on average in the TMD simulations and 42% complete on average in the RP-TMD simulations. At this point, the structural changes in loop L16 were even further from

Table 2. Completion of the Lip and L16 Refolding at the Time of Maximum Domain Closure in the TMD and RP-TMD Simulations[a]

system	lip (%)	loop L16 (%)
TMD[b]	44 ± 18	30 ± 15
RP-TMD[b]	42 ± 11	11 ± 9
TMD[c]	5	7
restrained TMD[d]	11	29

[a]The percentages are based on the rmsd values with the active state. At 0% completion, the rmsd with the active state is 7.98 Å for the lip and 3.89 Å for L16; at 100% completion, the rmsd is zero. [b]In implicit water, averaged over 25 simulations. [c]In explicit water using CHARMM. [d]In explicit water using NAMD.

completion, with 30% average completion in the TMD simulation and 11% average completion in the RP-TMD simulation. These results indicate that domain closure occurred before the lip and loop L16 have refolded. It is significant that the RP-TMD simulation showed more independence among the events, with an earlier completion of the domain closure relative to the refolding of the lip and L16, because RP-TMD has been shown to give lower free energy pathways than the TMD method.[49]

The contact between D334 and Q64 (discussed above) was observed to grow in strength during all of our TMD and RP-TMD simulations as the activation lip and L16 loop refolded. The corresponding contacts between R68 and R170 with T183 were not observed because the phosphate groups were not included in the TMD simulations. To accelerate the calculations, the RP-TMD and TMD simulations (25 each) were performed with an implicit solvent model. To test whether the implicit solvent model affected the results, we repeated a TMD and a restrained TMD simulation in explicit water. Both simulations showed behavior similar to that of the implicit solvent simulations, with domain closure occurring well before the other structural changes. The simulations suggest that the domain closure happens early in the activation process (even earlier than in the implicit water simulations), with the refolding of the activation lip and loop L16 helping to stabilize the domain closure and lock the protein in the active conformation. Our results also help to explain the larger closure angle of monophosphorylated ERK1 (Table 1 and ref 24); in

that structure, the activation lip has not yet refolded to lock the domain closure, resulting in a larger angle. A movie of the transition is given as Supporting Information.

G83 Is Important for ERK2 Catalytic Activity. We observed significant differences in the Ramachandran map of G83 between the inactive and active states. In the active state simulations, G83 sampled much wider regions of the Ramachandran map than in the inactive state (Figure S5 of the Supporting Information). While the structural changes associated with this motion are small, we observed that it allowed the strengthening of contacts between the gatekeeper residue Q103 and G83 in the active state, including a hydrogen bond between the backbone carbonyl of G83 and the NE2 hydrogen bond donor of Q103. Furthermore, G83 is conserved in MAPK or MAPK activator proteins [ERK1 and -2, MEK1 and -2, and p38α and -δ (Figure S4 of the Supporting Information)]. On the basis of these observations, it was hypothesized that mutation of G83 to an alanine would inhibit the catalytic activity of the enzyme. Simulations of a G83A mutant demonstrated behavior very similar to that of the inactive state. Domain closure was absent in the G83A simulation (Table 1), and the correlation patterns corresponded to those of the inactive state (Table T2 and Figure S2 of the Supporting Information). The lip retained strong (anti)correlation with the rest of the protein and strong positive correlation with the DEF site as in the inactive state simulation. In addition, the Ramachandran map of the G83A mutant resembled that of the inactive state (Figure S5 of the Supporting Information). Accordingly, the G83A mutant was generated and assayed for phosphorylation activity and its ability to be phosphorylated compared to wild-type ERK. These experiments validated the importance of G83: mutating G83 to alanine completely abolished ERK's ability to phosphorylate MBP, while the ability of G83A to be phosphorylated by MEK1 was similar to that of the wild type (Figure 7).

The Mutated Hydrophobic Residues in ERK2 Resemble the Molecular Brake in FGFR2. In FGF receptor 2 (FGFR2), certain residues in the hinge (N549, E565, and K641) form strong hydrogen bonds that act as a molecular brake to prevent premature kinase activation.[54] Structural overlays of ERK2 and FGFR2 showed local overlap between the molecular brake residues of FGFR2 and the autophosphorylation pathway residues of ERK2. The structures were aligned on the basis of the backbone atoms in the C-terminal helices (helices D and E in ERK2) because our simulations indicated that these helices were not very flexible, thus providing a good reference point. Despite a large overall rmsd (11.1 Å for the N-domain and 10.4 Å for the C-domain), which is due to differences in the relative orientations of various structural elements, the alignment gave reasonable local overlap of the hinge regions of the kinases. In FGFR2, hydrogen bonds connecting N549, E565, and K641 rigidify the interface between the N- and C-domains; mutations that remove these hydrogen bonds lead to constitutive activation of the kinase.[54] The two bulky, hydrophobic ERK2 residues mutated in this study, I84 and L73, point directly into the corresponding domain interface in ERK2 (Figure 8), suggesting that removal of these bulky side chains from ERK2 allows premature (non-phosphorylation-dependent) closure of the N-domain, as observed in our simulations.

Another contact of interest in that region was that between K162 and I81. In the inactive state, the amino group of K162 formed a weak hydrogen bond with the backbone of I81; this hydrogen bond was significantly weakened in the mutants and

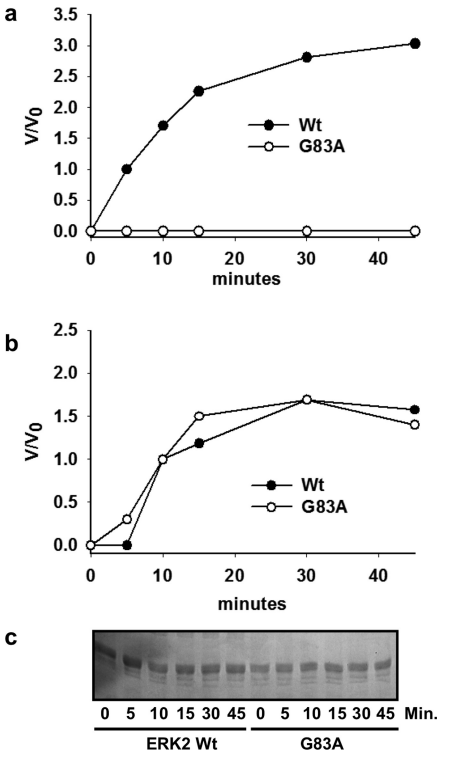

Figure 7. Enzymatic activity of the ERK2 G83A mutant. ERK2 wild type or G83A was incubated with constitutively active MKK1 and MBP as a substrate. (a) Incorporation of phosphate into MBP. (b) Incorporation of phosphate into ERK2 wild type or G83A. (c) ERK2 protein levels in kinase assays shown for panels a and b.

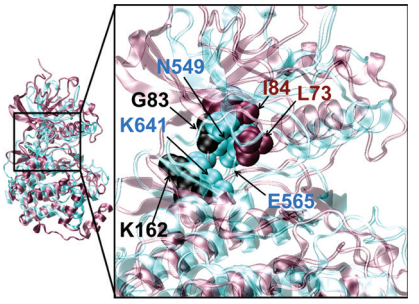

Figure 8. Structural overlay of the inactive states of the FGFR2 and ERK2 kinases. The structures were aligned on the basis of the C-terminal helices (helices D and E in ERK2). Despite large overall rmsds (see the text), the interface between the N- and C-domains was reasonably aligned. The FGFR2 structure is shown as cyan ribbons, with the molecular brake residues highlighted as cyan van der Waals spheres (N549, E565, and K641). The ERK2 structure is shown as magenta ribbons, with residues L73 and I84 shown as magenta spheres. K162 and G83, which were proposed for mutation in this study, are shown as black spheres.

absent in the active state. The conservation of K162 across the family of tyrosine kinases (Figure S4 of the Supporting Information) also suggested the importance of this residue.[55] Accordingly, it was predicted that the hydrogen bond of K162 contributes to ERK1 ands -2 activation, and a K162M mutation was prepared and tested experimentally. The mutation experiments showed that this contact does not contribute to activation, however, as the K162M mutant lacked activity (Figure 9). In addition, the mutant lost the ability to undergo

dx.doi.org/10.1021/bi200503a | Biochemistry 2011, 50, 8038–8048

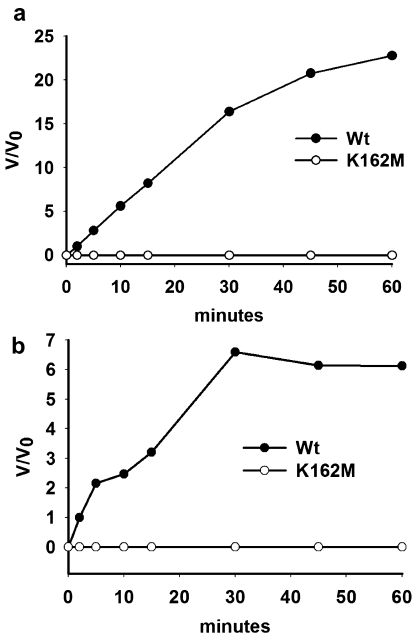

Figure 9. Loss of ERK2 enzymatic activity due to the K162M mutation. ERK2 wild type and K162M were incubated with MBP as a substrate for the times indicated. (a) Incorporation of phosphate into MBP. (b) Autophosphorylation of ERK2 wild type or K162M.

phosphorylation by MEK1. To rationalize the effects of this mutation, we performed MD simulations of the K162M mutant. In the simulation, minimal domain closure occurred (Table 1), which is consistent with our hypothesis that domain closure is required for autophosphorylation. Nevertheless, correlations involving the activation lip showed strong similarity to those of the active state (Figure S2 of the Supporting Information), and the MKI showed correlations between those of the active and inactive states. The experimental and simulation results indicate that K162 plays an important role in ERK function. Structural models suggest that this might be associated with the location of the residue on the surface of the protein adjacent to T157 and T158, which comprise the ED substrate docking site.

DISCUSSION

In contrast to predictions of the existing model for autoactivation of ERK2,[28] our simulations did not detect increased atomic fluctuations of the activation lip in the mutants. Instead, our simulations indicate that closure of the N-domain over the C-domain might be the determining factor for autoactivation of the kinase. Domain closure was observed in all mutant simulations; moreover, TMD simulations showed that domain closure occurred before the refolding of the activation lip or L16 loop. It is of particular interest that we also observed domain closure in the constitutively active R65S mutant, because the R65 residue is not involved in the proposed hydrophobic spine.[28] The quasi-harmonic analysis showed that domain closure aligns the hinge motion of the kinase over the active site, presumably allowing intramolecular autophosphorylation. The transfer entropy analysis indicated that in the domain-closed but not yet fully activated structures, the N-domain, and particularly helix C, drives fluctuations in the lip that may lead to activation.

Our results suggesting that autophosphorylation starts with domain closure, followed by the refolding of the activation lip to lock the kinase in its active conformation, are interesting in that this sequence of events might be different for other kinases. For example, computer simulations indicated that in the activation of Src kinase the activation lip refolds before domain closure.[56] The importance of domain closure for the autoactivation mechanism of ERK can also be inferred from the structure of monophosphorylated ERK1.[24] In this structure, domain closure has occurred, but the conformations of the activation and L16 loops are similar to those of the inactive state. However, monophosphorylated ERK1 has a basal activity, which is only 500-fold lower than that of the fully activated protein.

While domain closure appears to be sufficient to induce autophosphorylation of the kinase and a basal level of activity, dual phosphorylation is required for full functional activity.[28,57] Our results demonstrate an important role for the second phosphorylation event, by allowing pT183 to displace D334 and establish the hydrogen bond networks required to lock the kinase in the active conformation. In addition, our transfer entropy analysis indicates that the activation lip does not become a strong driver of the motion of the rest of the protein until both phosphorylation events have occurred.

Results from the simulations also indicated an important role for Q64 in folding of loop L16. The Q64C mutant was predicted to hinder the folding of loop L16 and disrupt the dimerization interface by removal of the strong Q64–D334 contact that is observed in all domain-closed states. Experimental data in native nondenaturing gels confirmed that the Q64C mutant migrated faster than the wild type, suggesting the absence of dimer formation and demonstrating the importance of the proper refolding of loop L16 for opening the dimerization interface and enzyme activity.

The conserved G83 residue sampled different areas of the Ramachandran map in the inactive state and in the active and autoactivated states. Because of these differences, contacts between G83 and the gatekeeper residue Q103 were strengthened in the active states. On the basis of these results, we predicted that the G83A mutant would deter activation of the kinase. This, indeed, turned out to be the case. Despite the G83A mutant being phosphorylated by the upstream MKK1, this ERK2 protein was unable to phosphorylate MBP.

Molecular overlays suggested a resemblance between the ERK2 autophosphorylation pathway residues and the residues involved in the molecular brake of the FGFR2[54] kinase. These residues are found in similar positions and affect the rigidity of the interface between the N- and C-domains. On the basis of the overlays and simulation result, K162 was hypothesized to play a role in ERK1 and -2 activation. A K162M mutant did not show autoactivation, however, but was incapable of achieving the active state, apparently because of its inability to be phosphorylated. Simulations showed domain closure also did not occur for K162M. While speculative, the K162M results might be associated with the location of K162 on the surface of the protein, and particularly by its location in a region adjacent to the ED docking domain.

ASSOCIATED CONTENT

Supporting Information

Movies of the hinge motion in the active and inactive states, the twisting motion of the active state, and the TMD transition pathway, figures of convergence tests, the variance–covariance matrices for the mutant and monophosphorylated states,

contact histograms for D334, sequence alignment of MAPKs, the free energy surface for backbone flexibility of G83, fluorescence spectra of ERK2 wild type and mutants to indicate structural integrity, and tables that list the solvent accessible surface of Y185 and mean correlation coefficients. This material is available free of charge via the Internet at http://pubs.acs.org.

AUTHOR INFORMATION

Corresponding Author

*A.v.d.V.: e-mail, avandervaart@usf.edu; phone, (813) 974-8762; fax, (813) 974-3203. A.D.M.: e-mail, alex@outerbanks.umaryland.edu; phone, (410) 706-7442; fax, (410) 706-5017. P.S.: e-mail, pshapiro@rx.umaryland.edu; phone, (410) 706-8522; fax, (410) 706-0346.

Present Address

[‖]Department of Chemistry and Biochemistry, Utica College, 1600 Burrstone Rd., Utica, NY 13502.

Funding

This work was supported by National Science Foundation CAREER Award CHE-1007816 to A.v.d.V. and National Institutes of Health Grant CA120215 to P.S. and A.D.M.

ACKNOWLEDGMENTS

Computer time for the work was provided by the TeraGrid, the Arizona State University Fulton High Performance Computing Initiative, and University of South Florida Research Computing. We thank Justin Spiriti and Hiqmet Kamberaj for technical assistance and Cheng Xu for preparatory simulations.

ABBREVIATIONS

MAPK, mitogen-activated protein kinase; ERK, extracellular signal-regulated kinase; MD, molecular dynamics; MKI, MAP kinase insertion; TMD, targeted molecular dynamics; RP-TMD, restricted perturbation targeted molecular dynamics.

REFERENCES

(1) Pimienta, G., and Pascual, J. (2007) Canonical and alternative MAPK signaling. *Cell Cycle 6*, 2628−2632.

(2) Chen, Z., Gibson, T. B., Robinson, F., Silvestro, L., Pearson, G., Xu, B. E., Wright, A., Vanderbilt, C., and Cobb, M. H. (2001) MAP kinases. *Chem. Rev. 101*, 2449−2476.

(3) Roux, P. P., and Blenis, J. (2004) ERK and p38 MAPK-activated protein kinases: A family of protein kinases with diverse biological functions. *Microbiol. Mol. Biol. Rev. 68*, 320−344.

(4) Bos, J. L. (1989) Ras oncogenes in human cancer: A review. *Cancer Res. 49*, 4682−4689.

(5) Malumbres, M., and Barbacid, M. (2003) Timeline—RAS oncogenes: The first 30 years. *Nat. Rev. Cancer 3*, 459−465.

(6) Malumbres, M., and Barbacid, M. (2003) Timeline—RAS oncogenes: The first 30 years. *Nat. Rev. Cancer 3*, 708.

(7) Burkhard, K., Smith, S., Deshmukh, R., MacKerell, A. D., and Shapiro, P. (2009) Development of Extracellular Signal-Regulated Kinase Inhibitors. *Curr. Top. Med. Chem. 9*, 678−689.

(8) Montagut, C., and Settleman, J. (2009) Targeting the RAF-MEK-ERK pathway in cancer therapy. *Cancer Lett. 283*, 125−134.

(9) Wong, K. K. (2009) Recent Developments in Anti-Cancer Agents Targeting the Ras/Raf/MEK/ERK Pathway. *Recent Pat. Anti-Cancer Drug Discovery 4*, 28−35.

(10) McCubrey, J. A., Milella, M., Tafuri, A., Martelli, A. M., Lunghi, P., Bonati, A., Cervello, M., Lee, J. T., and Steelman, L. S. (2008) Targeting the Raf/MEK/ERK pathway with small-molecule inhibitors. *Curr. Opin. Invest. Drugs 9*, 614−630.

(11) Roberts, P. J., and Der, C. J. (2007) Targeting the Raf-MEK-ERK mitogen-activated protein kinase cascade for the treatment of cancer. *Oncogene 26*, 3291−3310.

(12) Chen, F., Hancock, C. N., Macias, A. T., Joh, J., Still, K., Zhong, S., MacKerell, A. D. Jr., and Shapiro, P. (2006) Characterization of ATP-independent ERK inhibitors identified through in silico analysis of the active ERK2 structure. *Bioorg. Med. Chem. Lett. 16*, 6281−6287.

(13) Akella, R., Moon, T. M., and Goldsmith, E. J. (2008) Unique MAP Kinase binding sites. *Biochim. Biophys. Acta 1784*, 48−55.

(14) Kohno, M., and Pouyssegur, J. (2006) Targeting the ERK signaling pathway in cancer therapy. *Ann. Med. 38*, 200−211.

(15) Khan, T. K., and Alkon, D. L. (2006) An internally controlled peripheral biomarker for Alzheimer's disease: Erk1 and Erk2 responses to the inflammatory signal bradykinin. *Proc. Natl. Acad. Sci. U.S.A. 103*, 13203−13207.

(16) Matsushita, T., Chan, Y. Y., Kawanami, A., Balmes, G., Landreth, G. E., and Murakami, S. (2009) Extracellular Signal-Regulated Kinase 1 (ERK1) and ERK2 Play Essential Roles in Osteoblast Differentiation and in Supporting Osteoclastogenesis. *Mol. Cell. Biol. 29*, 5843−5857.

(17) Canagarajah, B. J., Khokhlatchev, A., Cobb, M. H., and Goldsmith, E. J. (1997) Activation Mechanism of the MAP Kinase ERK2 by Dual Phosphorylation. *Cell 90*, 859−869.

(18) Haystead, T. A. J., Dent, P., Wu, J., Haystead, C. M. M., and Sturgill, T. W. (1992) Ordered phosphorylation of p42(MAPK) by MAP kinase kinase. *FEBS Lett. 306*, 17−22.

(19) Burack, W. R., and Sturgill, T. W. (1997) The activating dual phosphorylation of MAPK by MEK is nonprocessive. *Biochemistry 36*, 5929−5933.

(20) Ferrell, J.E., and Bhatt, R. R. (1997) Mechanistic studies of the dual phosphorylation of mitogen-activated protein kinase. *J. Biol. Chem. 272*, 19008−19016.

(21) Cobb, M. H., and Goldsmith, E. J. (2000) Dimerization in MAP-kinase signaling. *Trends Biochem. Sci. 25*, 7−9.

(22) Turjanski, A. G., Vaque, J. P., and Gutkind, J. S. (2007) MAP kinases and the control of nuclear events. *Oncogene 26*, 3240−3253.

(23) Zhang, F., Strand, A., Robbins, D., Cobb, M. H., and Goldsmith, E. J. (1994) Atomic structure of the MAP kinase ERK2 at 2.3 Å resolution. *Nature 367*, 704−711.

(24) Kinoshita, T., Yoshida, I., Nakae, S., Okita, K., Gouda, M., Matsubara, M., Yokota, K., Ishiguro, H., and Tada, T. (2008) Crystal structure of human mono-phosphorylated ERK1 at Tyr204. *Biochem. Biophys. Res. Commun. 377*, 1123−1127.

(25) Tanoue, T., Maeda, R., Adachi, M., and Nishida, E. (2000) Identification of a docking groove on ERK and p38 MAP kinases that regulates the specificity of docking interactions. *EMBO J. 20*, 466−479.

(26) Tanoue, T., Adachi, M., Moriguchi, T., and Nishida, E. (2000) A conserved docking motif in MAP kinases common to substrates, activators and regulators. *Nat. Cell Biol. 2*, 110−116.

(27) Lee, T., Hoofnagle, A. N., Kabuyama, Y., Stroud, J., Min, X., Goldsmith, E. J., Chen, L., Resing, K. A., and Ahn, N. G. (2004) Docking Motif Interactions in MAP Kinases Revealed by Hydrogen Exchange Mass Spectrometry. *Mol. Cell 14*, 43−55.

(28) Emrick, M. A., Lee, T., Starkey, P. J., Mumby, M. C., Resing, K. A., and Ahn, N. G. (2006) The gatekeeper residue controls autoactivation of ERK2 via a pathway of intramolecular connectivity. *Proc. Natl. Acad. Sci. U.S.A. 103*, 18101−18106.

(29) Levin-Salomon, V., Kogan, K., Ahn, N. G., Livnah, O., and Engelberg, D. (2008) Isolation of Intrinsically Active (MEK-independent) Variants of the ERK Family of Mitogen-activated Protein (MAP) Kinases. *J. Biol. Chem. 283*, 34500−34510.

(30) Brooks, B. R., Brooks, C. L. III, MacKerell, A. D. Jr., Nilsson, L., Petrella, R. J., Roux, B., Won, Y., Archontis, G., Bartels, C., Boresch, S., Caflisch, A., Caves, L., Cui, Q., Dinner, A. R., Feig, M., Fischer, S., Gao, J., Hodoscek, M., Im, W., Kuczera, K., Lazaridis, T., Ma, J., Ovchinnikov, V.,

Paci, E., Pastor, R. W., Post, C. B., Pu, J. Z., Schaefer, M., Tidor, B., Venable, R. M., Woodcock, H. L., Wu, X., Yang, W., York, D. M., and Karplus, M. (2009) CHARMM: The biomolecular simulation program. *J. Comput. Chem. 30*, 1545−1614.

(31) Phillips, J. C., Braun, R., Wang, W., Gumbart, J., Tajkhorshid, E., Villa, E., Chipot, C., Skeel, R. D., Kale, L., and Schulten, K. (2005) Scalable molecular dynamics with NAMD. *J. Comput. Chem. 26*, 1781−1802.

(32) Michaud-Agrawal, N., Denning, E. J., Woolf, T. B., and Beckstein, O. (2011) MDAnalysis: A toolkit for the analysis of molecular dynamics simulations. *J. Comput. Chem.*, DOI: doi: 10.1002/jcc.21787.

(33) Humphrey, W., Dalke, A., and Schulten, K. (1996) VMD: Visual Molecular Dynamics. *J. Mol. Graphics 14*, 33−38.

(34) Frishman, D., and Argos, P. (1995) Knowledge-Based Protein Secondary Structure Assignment. *Proteins 23*, 566−579.

(35) Jorgensen, W., Chandrasekar, J., Madura, J., Impey, R., and Klein, M. (1983) Comparison of Simple Potential Functions for Simulating Liquid Water. *J. Chem. Phys. 79*, 926−935.

(36) MacKerell, A. D. Jr., Bashford, D., Bellot, M., Dunbrack, R. L. Jr., Evanseck, J. D., Field, M. J., Fischer, S., Gao, J., Guo, H., Ha, S., Joseph-McCarthy, D., Kuchnir, L., Kuczera, K., Lau, F. T. K., Mattos, C., Michnick, S., Ngo, T., Nguyen, D. T., Prodhom, B., Reiher, W. E. III, Roux, B., Schlenkrich, M., Smith, J. C., Stote, R., Straub, J., Watanabe, M., Wiórkiewicz-Kuczera, J., Yin, D., and Karplus, M. (1998) All-atom empirical potential for molecular modeling and dynamics studies of proteins. *J. Phys. Chem. B 102*, 3586−3616.

(37) MacKerell, A. D. Jr., Feig, M., and Brooks, C. L. III (2004) Extending the treatment of backbone energetics in protein force fields: Limitations of gas-phase quantum mechanics in reproducing protein conformational distributions in molecular dynamics simulations. *J. Comput. Chem. 25*, 1400−1415.

(38) Ryckaert, J. P., Ciccotti, G., and Berendsen, H. J. C. (1977) Numerical integration of the Cartesian equations of motion of a system with constraints: Molecular dynamics of n-alkanes. *J. Comput. Phys. 23*, 327−341.

(39) Essmann, U., Perera, L., Berkowitz, M., Darden, T., Lee, H., and Pedersen, L. G. (1995) A smooth particle mesh Ewald method. *J. Chem. Phys. 103*, 8577−8593.

(40) Larkin, M. A., Blackshields, G., Brown, N. P., Chenna, R., McGettigan, P. A., McWilliam, H., Valentin, F., Wallace, I. M., Wilm, A., Lopez, R., Thompson, J. D., Gibson, T. J., and Higgins, D. G. (2007) Clustal W and Clustal X version 2.0. *Bioinformatics 23*, 2947−2948.

(41) Ichiye, T., and Karplus, M. (1991) Collective motions in proteins: A covariance analysis of atomic fluctuations in molecular dynamics and normal mode simulations. *Proteins 11*, 205−217.

(42) Teeter, M. M., and Case, D. A. (1990) Harmonic and quasiharmonic descriptions of crambin. *J. Phys. Chem. 94*, 8091−8097.

(43) Karplus, M., and Kushick, J. N. (1981) Method for estimating the configurational entropy of macromolecules. *Macromolecules 14*, 325−332.

(44) Lange, O. F., and Grubmüller, H. (2006) Generalized correlation for biomolecular dynamics. *Proteins 62*, 1053−1061.

(45) Kamberaj, H., and van der Vaart, A. (2009) Extracting the causality of correlated motions from molecular dynamics simulations. *Biophys. J. 97*, 1747−1755.

(46) Frenkel, D., and Smit, B. (2002) *Understanding Molecular Simulation*, Academic Press, New York.

(47) Kamberaj, H., and van der Vaart, A. (2009) Correlated motions and interactions at the onset of the DNA-induced partial unfolding of Ets-1. *Biophys. J. 96*, 1307−1317.

(48) Schlitter, J., Engels, M., Krüger, P., Jacoby, E., and Wollmer, A. (1993) Targeted molecular dynamics simulation of conformational change: Application to the T ↔ R transition in insulin. *Mol. Simul. 10*, 291−308.

(49) van der Vaart, A., and Karplus, M. (2005) Simulation of conformational transitions by the restricted perturbation: Targeted molecular dynamics method. *J. Chem. Phys. 122*, 114903.

(50) Haberthür, U., and Caflisch, A. (2008) FACTS: Fast analytical continuum treatment of solvation. *J. Comput. Chem. 29*, 701−715.

(51) Mansour, S. J., Candia, J. M., Matsuura, J. E., Manning, M. C., and Ahn, N. G. (1996) Interdependent Domains Controlling the Enzymatic Activity of Mitogen-Activated Protein Kinase Kinase 1. *Biochemistry 35*, 15529−15536.

(52) Pargellis, C., Tong, L., Churchill, L., Cirillo, P. F., Gilmore, T., Graham, A. G., Grob, P. M., Hickey, E. R., Moss, N., Pav, S., and Regan, J. (2002) Inhibition of p38 MAP kinase by utilizing a novel allosteric binding site. *Nat. Struct. Biol. 9*, 268−272.

(53) Tanoue, T., and Nishida, E. (2003) Molecular recognitions in the MAP kinase cascades. *Cell. Signalling 15*, 455−462.

(54) Chen, H., Ma, J., Li, W., Eliseenkova, A. V., Xu, C., Neubert, T. A., Miller, W. T., and Mohammadi, M. (2007) A Molecular Brake in the Kinase Hinge Region Regulates the Activity of Receptor Tyrosine Kinases. *Mol. Cell 27*, 717−730.

(55) Hanks, S. K., Quinn, A. M., and Hunter, T. (1988) The protein kinase family: Conserved features and deduced phylogeny of the catalytic domains. *Science 241*, 42−52.

(56) Gan, W., Yang, S., and Roux, B. (2009) Atomistic view of the conformational activation of Src kinase using the string method with swarms-of-trajectories. *Biophys. J. 97*, L8−L10.

(57) Yao, Z., Dolginov, Y., Hanoch, T., Yung, Y. V., Ridner, G., Lando, Z., Zharhary, D., and Seger, R. (2000) Detection of partially phosphorylated forms of ERK by monoclonal antibodies reveals spatial regulation of ERK activity by phosphatases. *FEBS Lett. 468*, 37−42.